



# Optical properties of (GaAs/InAs)–GaAs<sub>y</sub>Sb<sub>1–y</sub> digital alloy superlattices in the short-wavelength infrared region calculated by an $sp^3d^5s^*$ tight-binding method

Takashi Kato<sup>1</sup> · Satofumi Souma<sup>2</sup>

Received: 4 March 2023 / Accepted: 13 April 2023 / Published online: 18 May 2023  
© The Author(s), under exclusive licence to Springer-Verlag GmbH, DE part of Springer Nature 2023

## Abstract

Ga<sub>x</sub>In<sub>1–x</sub>As–GaAs<sub>y</sub>Sb<sub>1–y</sub> type-II superlattices (T2SLs) have recently received broad attention as an InP-based optical absorption layer in short-wavelength infrared detectors. However, the cut-off wavelength of a GaInAs–GaAsSb T2SL detector is ordinarily around 2.4 μm at room temperature. This paper proposes extending the cut-off wavelength using a GaAs/InAs digital alloy instead of a Ga<sub>x</sub>In<sub>1–x</sub>As random alloy layer in a Ga<sub>x</sub>In<sub>1–x</sub>As–GaAs<sub>y</sub>Sb<sub>1–y</sub> T2SL. The calculation result employing an empirical  $sp^3d^5s^*$  tight-binding method has revealed that a (GaAs/InAs)–GaAs<sub>y</sub>Sb<sub>1–y</sub> digital alloy T2SL on an InP substrate possesses a band gap corresponding to a wavelength of 2.9 μm which is over 0.4 μm longer than that in a conventional GaInAs–GaAsSb T2SL at a temperature of 200 K. Figured optical absorption coefficient spectra of certain digital alloy T2SLs, e.g., a [(GaAs)<sub>4</sub>(InAs)<sub>4</sub>]<sub>2</sub>–(GaAs<sub>0.53</sub>Sb<sub>0.47</sub>)<sub>17</sub> structure, present a considerable polarization-direction dependence—originating from the asymmetrical shape of the wavefunction in the quantum well. Yet, by altering the atomic layer configuration in the growth direction of the digital alloy T2SL to have such a quantum well structure with a reflection symmetry as in [(GaAs)<sub>4</sub>(InAs)<sub>4</sub>]<sub>2</sub>(GaAs)<sub>3</sub>–(GaAs<sub>0.45</sub>Sb<sub>0.55</sub>)<sub>17</sub>, the polarization dependency can be dramatically decreased due to the symmetry improvement of the wavefunction.

**Keywords** Type-II superlattice · Digital alloy · Tight-binding · Absorption coefficient

## 1 Introduction

There are many attractive optical applications for industrial and medical uses in the short-wavelength infrared (SWIR) region (usually in the 1–3 μm wavelength range) [1–4]. As an example, the absorption wavelength regions for blood sugar (glucose) and proteins exist in the 2–2.5 μm wavelength range. Considering applications in the field of health-care, it is crucial to extend the cut-off wavelength while maintaining high sensitivity in the detector to that wavelength region. This report proposes adopting a digital alloy superlattice that enables the realization of a high-sensitivity photodetector even in the 2.5 μm wavelength region, where

difficulty exists to obtain sufficient sensitivity with a conventional type-II superlattice (T2SL) as described later. In the SWIR range, Hg<sub>x</sub>Cd<sub>1–x</sub>Te detectors possess a high quantum efficiency; yet, they have disadvantages such as comprising hazardous Hg and Cd heavy metals and being inferior in compositional uniformity for application in focal plane arrays [5, 6]. An alternative detector with an optical absorption layer of bulk Ga<sub>x</sub>In<sub>1–x</sub>As grown on an InP substrate has a cut-off wavelength of about 2.6 μm at room temperature, adopting a compressive strain (around 2 %) in the GaInAs layer [7]. Adding a much greater strain on the GaInAs layer to lengthen the gap wavelength ( $\lambda_g$ )—a wavelength equivalent to the band gap energy—may induce more defects in the epilayers and cause an increase in the dark current of the detector. Another study in a SWIR detector has reported that a Ga<sub>x</sub>In<sub>1–x</sub>As–GaAs<sub>y</sub>Sb<sub>1–y</sub> T2SL, whose lattice constant was matched to an InP substrate, attained a cut-off wavelength of around 2.4 μm at room temperature [8–11]. Regarding GaInAs–GaAsSb T2SL, as illustrated in Fig. 1, the  $\lambda_g$  can extend above 2.5 μm; however, the absorption coefficient rapidly decreases near the band gap. More specifically, as the

✉ Takashi Kato  
kato-takashi@sei.co.jp

<sup>1</sup> Transmission Devices Laboratory, Sumitomo Electric Industries, Ltd., Yokohama 244-8588, Japan

<sup>2</sup> Department of Electrical and Electronic Engineering, Kobe University, Kobe 657-8501, Japan

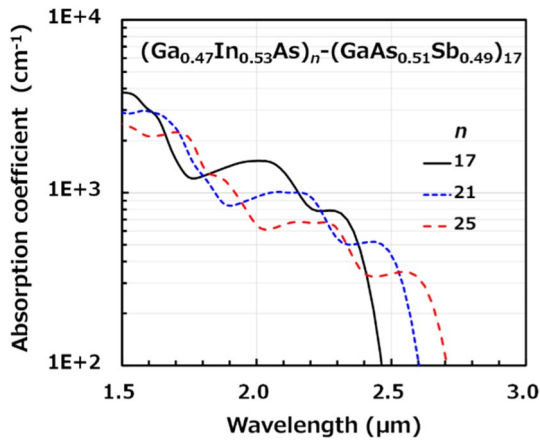


**Fig. 1** Absorption coefficient spectra in  $(\text{Ga}_{0.46}\text{In}_{0.54}\text{As})_n-(\text{GaAs}_{0.51}\text{Sb}_{0.49})_{17}$  T2SL on an (001) InP substrate at a temperature of 200 K.  $n$  denotes the GaInAs monolayer number. The above calculation using an empirical  $sp^3d^5s^*$  tight-binding method described in Sect. 2 is for incident light in the  $z$ -direction with [100] polarization

width of the electron well (GaInAs) layer increases, the  $\lambda_g$  of the T2SL becomes longer owing to lowering of the confined electron energy in the electron well layer. As a trade-off, the absorption coefficient near the band gap promptly decreases due to a reduction in the overlap of the wavefunctions of the conduction and valence bands.

This paper proposes extending the cut-off wavelength using a GaAs/InAs digital alloy (namely, a quantum well structure consisting of thin GaAs and InAs layers) instead of a  $\text{Ga}_x\text{In}_{1-x}\text{As}$  random alloy layer in a  $\text{Ga}_x\text{In}_{1-x}\text{As}-\text{GaAs}_y\text{Sb}_{1-y}$  T2SL. Regarding the application of digital alloys to photodetectors, several studies, especially in avalanche photodiodes, have demonstrated that the ionization ratio can be improved [12, 13]. Another study on digital alloys as

a photodiode has suggested adopting a GaAs/InAs digital alloy instead of a bulk  $\text{Ga}_x\text{In}_{1-x}\text{As}$  absorption layer which might enable the cut-off wavelength to lengthen from 1.7  $\mu\text{m}$  to greater than 1.9  $\mu\text{m}$  (although the quantum efficiency reduces from approximately 95 % to 60 % at a wavelength of 1.5  $\mu\text{m}$ ) [14]. However, few studies have attempted to apply digital alloys to  $\text{Ga}_x\text{In}_{1-x}\text{As}-\text{GaAs}_y\text{Sb}_{1-y}$  T2SLs. Figure 2 illustrates a schematic diagram of the energy band alignment of a digital alloy  $(\text{GaAs}/\text{InAs})-\text{GaAs}_y\text{Sb}_{1-y}$  superlattice and a conventional  $\text{Ga}_x\text{In}_{1-x}\text{As}-\text{GaAs}_y\text{Sb}_{1-y}$  T2SL. In the digital alloy superlattice, as shown in Sect. 3, the conduction and the valence band wavefunction of the superlattice are mainly confined in the GaAs/InAs and the  $\text{GaAs}_y\text{Sb}_{1-y}$  layers, respectively, which implies the superlattice belongs to the T2SL structure. This paper shows, for the first time, using an empirical  $sp^3d^5s^*$  tight-binding (TB) method, an InP-based  $(\text{GaAs}/\text{InAs})-\text{GaAs}_y\text{Sb}_{1-y}$  digital alloy T2SL that has a longer  $\lambda_g$  of 2.9  $\mu\text{m}$  at a temperature ( $T$ ) of 200 K while preserving a high absorption coefficient near the band gap.

Turning to another aspect of the optical properties of T2SLs, a previous study on the polarization-direction dependency of the dipole matrix elements in InAs–GaSb T2SL systems suggested the following [15]: If an InAs–GaSb T2SL system has a  $C_{2v}$  point group symmetry, the dipole matrix elements show anisotropy for [110]- and  $[-110]$ -polarized incident light. On the other hand, in an InAs–GaSb T2SL system with a  $D_{2d}$  point group symmetry, dipole matrix elements present no dependence on polarization directions. Concerning digital alloy T2SLs, however, little attention has been paid to optical anisotropy. This study discusses the dependency of the absorption coefficient on the polarization direction of incident light in  $(\text{GaAs}/\text{InAs})-\text{GaAs}_y\text{Sb}_{1-y}$  digital alloy T2SLs and reveals that a digital alloy T2SL with a symmetrical quantum well structure

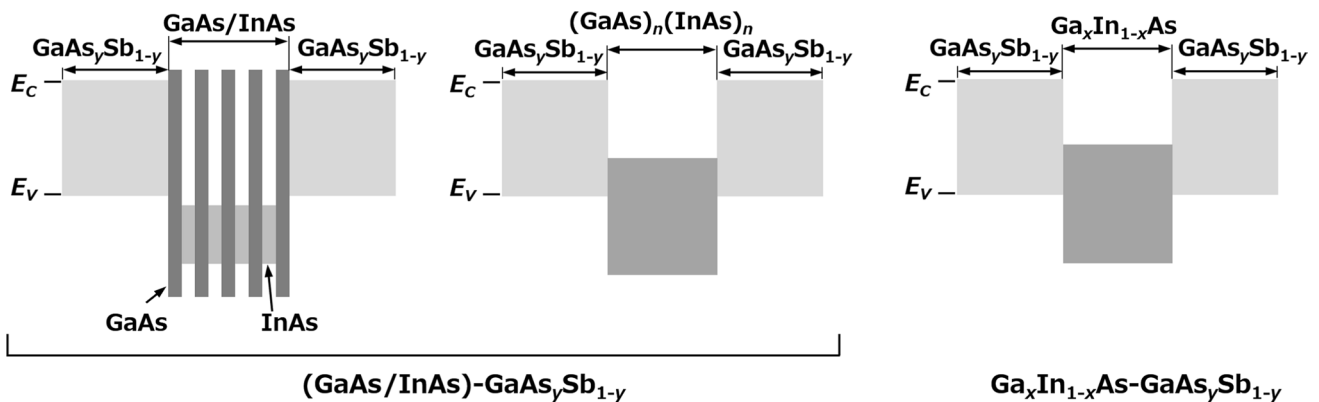


**Fig. 2** Schematic figures showing the band alignment of a  $(\text{GaAs}/\text{InAs})-\text{GaAs}_y\text{Sb}_{1-y}$  superlattice (left and middle) and a  $\text{Ga}_x\text{In}_{1-x}\text{As}-\text{GaAs}_y\text{Sb}_{1-y}$  T2SL (right side). In the middle figure, as an example, the GaAs/InAs layer of the  $(\text{GaAs}/\text{InAs})-\text{GaAs}_y\text{Sb}_{1-y}$  superlattice is regarded as one material of a superlattice of  $(\text{GaAs})_n(\text{InAs})_n$ . Each

gray rectangle depicts the band gap energy region of the layer, the lower and the upper side position of which show the energy levels of the valence band maximum ( $E_v$ ) and the conduction band minimum ( $E_c$ ), respectively

decreases the polarization dependency drastically owing to the ameliorated symmetry of the wavefunction.

## 2 Calculation methods

An empirical nearest-neighbor  $sp^3d^5s^*$  TB approximation under periodic boundary conditions was used to investigate the electronic structures and the optical absorption properties in T2SLs. Employed TB parameters for the binary and alloy semiconductors were derived from the calculated band structures of the binary compounds by the hybrid quasiparticle self-consistent GW method [16]. Postulating that the growth of the T2SL on a (001) InP substrate along the  $z$ -direction is pseudomorphic in our calculation model, the classical elasticity theory may determine the position of atoms in the T2SL [17]; thus, the TB parameters have been corrected for the resulting lattice strain by using the generalized Harrison's  $d^{-2}$  law [18]. The  $\text{Ga}_x\text{In}_{1-x}\text{As}$  TB parameters related to the cation would characterize the (virtual) cation atoms in the alloy on the supposition that the Ga and In atoms are randomly distributed on the cation sites in the  $\text{Ga}_x\text{In}_{1-x}\text{As}$  layer; anion atoms in the  $\text{GaAs}_y\text{Sb}_{1-y}$  layer are likewise distributed. In the (GaAs/InAs)<sub>n</sub>–GaAs<sub>y</sub>Sb<sub>1–y</sub> digital alloy T2SL, the composition value  $y$  in the  $\text{GaAs}_y\text{Sb}_{1-y}$  layer was determined so that the average strain in the  $z$ -direction was zero within the one period of the T2SL. To illuminate the differences in the electron quantum well layer—the  $\text{Ga}_x\text{In}_{1-x}\text{As}$  or the GaAs/InAs digital alloy layer, the thickness of the  $\text{GaAs}_y\text{Sb}_{1-y}$  electron barrier layer was fixed at 17 monolayers (about 5.0 nm) in all the calculated T2SL structures. The optical absorption spectra of T2SLs were calculated based on Fermi's golden rule by the same method in a previous work [19], with the conditions that a linearly polarized light enters along the  $z$ -direction and at  $T=200$  K.

## 3 Results and discussion

### 3.1 [(GaAs)<sub>n</sub>(InAs)<sub>m</sub>]<sub>k</sub>–(GaAs<sub>y</sub>Sb<sub>1–y</sub>)<sub>l</sub> T2SLs

First, the study compares a conventional  $(\text{Ga}_{0.47}\text{In}_{0.53}\text{As})_{17}-(\text{GaAs}_{0.51}\text{Sb}_{0.49})_{17}$  T2SL (hereafter abbreviated as GaInAs–GaAsSb) to two simple digital alloy T2SLs— $[(\text{GaAs})_2(\text{InAs})_2]_4-(\text{GaAs}_{0.52}\text{Sb}_{0.48})_{17}$  and  $[(\text{GaAs})_4(\text{InAs})_4]_2-(\text{GaAs}_{0.53}\text{Sb}_{0.47})_{17}$  (hereafter referred to as DA1 and DA2, respectively). Regarding the averaged compositions of Ga and In in the GaAs/InAs digital alloy layers in DA1 and DA2, each digital alloy is equivalent to a random alloy  $\text{Ga}_{0.50}\text{In}_{0.50}\text{As}$ . The thicknesses of the GaAs/InAs digital alloy layers in one period of DA1 and DA2 are 4.7 nm, which is a little thinner than a  $(\text{Ga}_{0.47}\text{In}_{0.53}\text{As})_{17}$  layer thickness of 5.0 nm.

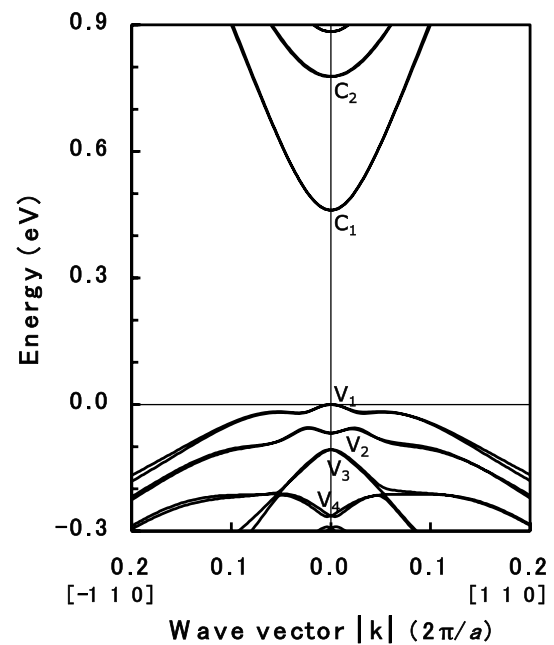


**Fig. 3** Energy dispersion  $E(\mathbf{k})$  of DA1 near the  $\Gamma$ -point along the  $[-110]$  and the  $[110]$  direction;  $C_1$  and  $C_2$  denote the first and the second conduction sub-band, respectively;  $V_1$ – $V_4$  indicates the first to the fourth valence sub-band in order. Each sub-band with two spin states degenerates at the  $\Gamma$ -point

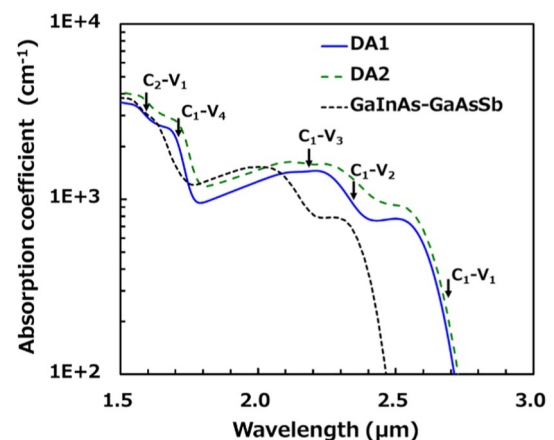


**Fig. 4** Absorption coefficient spectra of DA1, DA2, and GaInAs–GaAsSb for  $[100]$ -polarized incident light. The arrows indicate the wavelength corresponding to each transition energy at the  $\Gamma$ -point between the sub-bands of DA1 depicted in Fig. 3

At the outset, to see the band structure of the (GaAs/InAs)<sub>n</sub>–GaAsSb digital alloy T2SL and use it for identifying the onsets of the optical transition energies between the sub-bands in the conduction and the valence band, Fig. 3 presents the energy dispersion  $E(\mathbf{k})$  of DA1 calculated in the neighborhood of the  $\Gamma$ -point as an example. Figure 4 presents the calculated absorption coefficient spectra of GaInAs–GaAsSb, DA1, and DA2 for the  $[100]$ -polarized

incident light; the  $\lambda_g$ s of these T2SLs are 2.45, 2.69, and 2.70  $\mu\text{m}$ , respectively. The spectra suggest that the digital alloys can be utilized for lengthening the cut-off wavelength in SWIR detectors.

Concerning the absorption coefficient dependence on the polarization directions of the incident light in the digital alloy T2SLs, Fig. 5a and b reveal the traits in DA1 and DA2, respectively. The polarization dependency in the DA2 spectra is more notable than that in the DA1 ones, which, with conjecture from anisotropy studies on the influence of the interface layers in InAs–GaSb T2SL systems [15], presumably relates to the asymmetry of the band-offset shape along the  $z$ -direction. Figure 6a and b illustrate, for DA1 and DA2, respectively, the valence band-offset (VBO) and the conduction band-offset (CBO)

distribution, together with the squared modulus of the wavefunction at the valence band maximum (VBM) and the conduction band minimum (CBM). Due to the prominent asymmetry of the CBO in DA2 shown in Fig. 6b, the wavefunction at the CBM shifts the position accordingly, and its magnitude increases towards the right-side interface ( $\text{IF}_2$ ) of the digital alloy layer. Thus, the atomic configuration near the  $\text{IF}_2$  in Fig. 6b affects the optical-transition-matrix elements to a greater extent than in the neighborhood of the left interface ( $\text{IF}_1$ ). It suggests that, in the absorption coefficient, the asymmetrical shape of the wavefunction gives rise to dependence on the polarization direction of the incident light, which this report discusses in the next section.

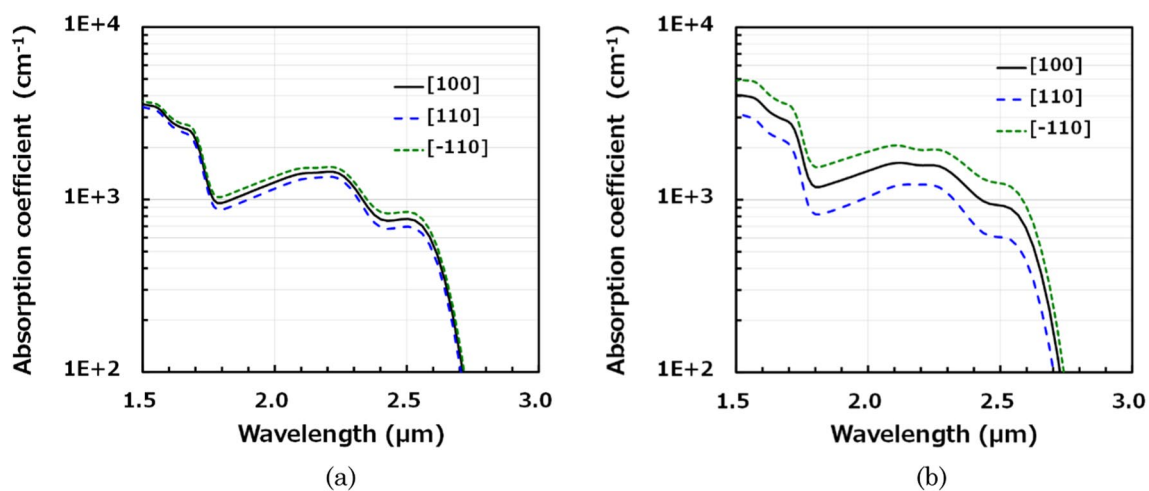


Fig. 5 Dependences of the absorption coefficients on polarization directions in **a** DA1 and **b** DA2

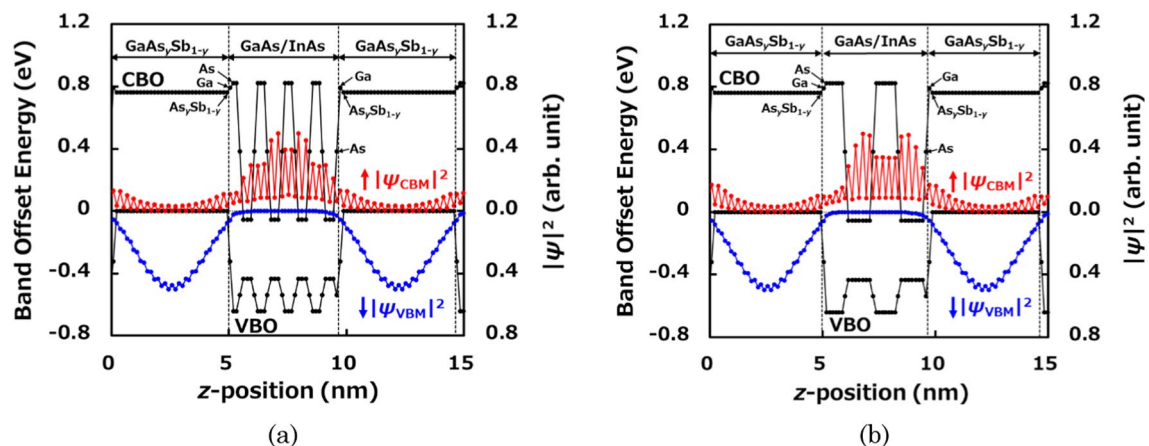


Fig. 6 Distributions of the VBO and the CBO in **a** DA1 and **b** DA2; and the squared modulus of the wavefunction at the VBM and the CBM. Closed circles indicate the positions of atoms; lines between the atomic sites are to guide the eye. "As $_y$ Sb $_{1-y}$ " denotes the anion

atom of GaAs $_y$ Sb $_{1-y}$  in the TB scheme.  $\text{IF}_1$  and  $\text{IF}_2$  designate the positions of each interface between the GaAs/InAs digital alloy and the GaAs $_y$ Sb $_{1-y}$  electron barrier layers

### 3.2 Symmetrical digital alloy T2SLs

The following is an exploration of symmetrical T2SLs to investigate the mechanism of the variation of the absorption coefficient according to the polarization direction of incident light and the influence of the symmetry of the wavefunction on the absorption coefficient in digital alloy T2SLs. Here, this paper defines the term “symmetrical T2SL” as a T2SL having a reflection symmetry in the *z*-direction atomic plane row. As an example of a symmetrical (GaAs/InAs)-GaAs<sub>y</sub>Sb<sub>1-y</sub> digital alloy T2SL, Fig. 7 schematically represents an atomic plane row along the *z*-direction of [(GaAs)<sub>2</sub>(InAs)<sub>2</sub>]<sub>4</sub>(GaAs)-(GaAs<sub>y</sub>Sb<sub>1-y</sub>)<sub>l</sub> T2SL.

In still other examples, the following structures of (GaAs/InAs)-GaAs<sub>y</sub>Sb<sub>1-y</sub> digital alloy T2SL are symmetrical:

$$\{(\text{GaAs})_{n'}(\text{InAs})_m[(\text{GaAs})_n(\text{InAs})_m]_k(\text{GaAs})_{n'-1}\} - (\text{GaAs}_y\text{Sb}_{1-y})_l, \tag{1}$$

where  $n, n', m, l \in \mathbb{N}; k \in \mathbb{N}_0$ .

Subsequently, modifying the prior asymmetrical DA1 and DA2 structures, we examined the following two symmetrical digital alloy T2SLs:  $\{[(\text{GaAs})_2(\text{InAs})_2]_4(\text{GaAs})\} - (\text{GaAs}_{0.49}\text{Sb}_{0.51})_{17}$  and  $\{[(\text{GaAs})_4(\text{InAs})_4]_2(\text{GaAs})_3\} - (\text{GaAs}_{0.45}\text{Sb}_{0.55})_{17}$  (hereafter referred to

as SDA1 and SDA2, respectively). Figure 8a and b show the VBO and the CBO distributions and the squared modulus of the wavefunction at the VBM and the CBM in SDA1 and SDA2, respectively. As shown in these Figures, the VBO and CBO of the SDA1 and SDA2 have a mirror-symmetrical profile, which brings about the symmetrical shapes relating to the magnitude of each wavefunction.

Figure 9a and b present the absorption coefficient spectra, depending on the polarization directions of the incident light in SDA1 and SDA2, respectively. The variation of the absorption coefficient conforming to the difference in the polarization direction decreases outstandingly in both symmetrical T2SLs. The  $\lambda_g$ s of SDA1 and SDA2 are 2.84 and 3.19  $\mu\text{m}$ , respectively, being longer than those in each of DA1 and DA2, probably due to the thicker electron well (GaAs/InAs digital alloy) layers.

In the following, this paper will elucidate the cause of the polarization-direction dependency of the absorption coefficient in asymmetrical T2SLs. Two simple examples of short-period digital alloy T2SLs were prepared for the explanation: One was an asymmetrical (GaAs)<sub>2</sub>(InAs)<sub>2</sub>-(GaAs<sub>y</sub>Sb<sub>1-y</sub>)<sub>4</sub> T2SL, and the other was a symmetrical (GaAs)<sub>2</sub>(InAs)<sub>2</sub>(GaAs)-(GaAs<sub>y</sub>Sb<sub>1-y</sub>)<sub>3</sub> T2SL. Figure 10a and b show the atomic configuration in the

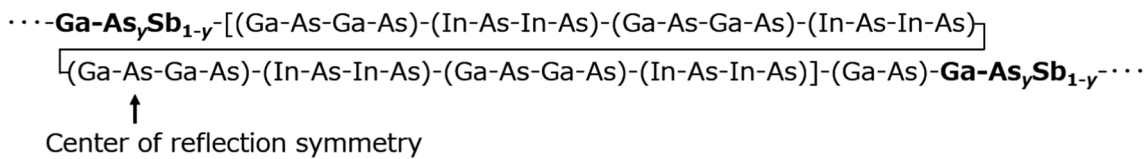


**Fig. 7** The *z*-direction row of the atomic plane (here, the symbol for an element represents its atomic plane), being in an *x-y* plane, in [(GaAs)<sub>2</sub>(InAs)<sub>2</sub>]<sub>4</sub>(GaAs)-(GaAs<sub>y</sub>Sb<sub>1-y</sub>)<sub>l</sub> T2SL. Bold letters represent the atomic planes in the *l*-monolayer of GaAs<sub>y</sub>Sb<sub>1-y</sub>; “As<sub>y</sub>Sb<sub>1-y</sub>”

in the figure means the anion of GaAs<sub>y</sub>Sb<sub>1-y</sub> in the TB scheme. The position of the As plane indicated by the arrow is the center of the reflection symmetry in the atomic plane row

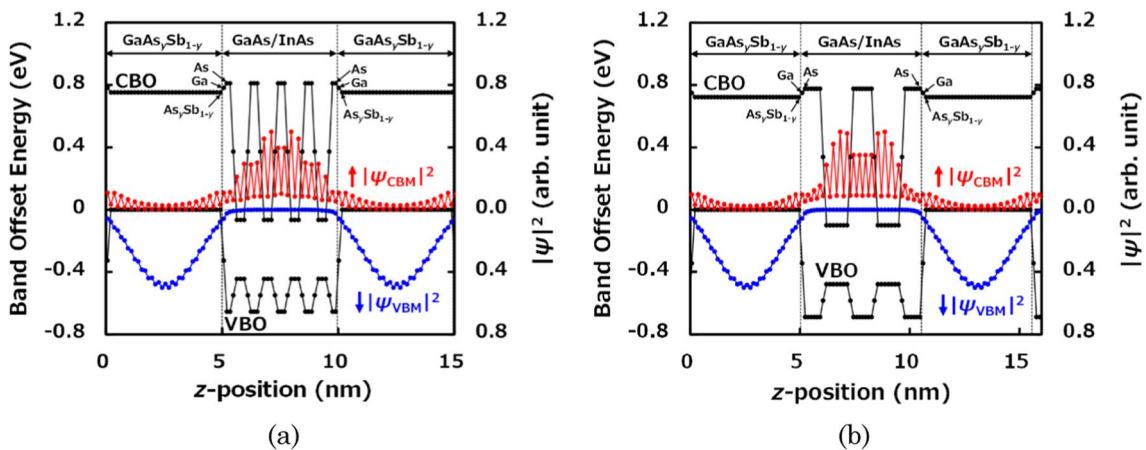


**Fig. 8** Distributions of VBO and CBO in **a** SDA1 and **b** SDA2; also, the squared modulus of the wavefunction at the VBM and the CBM are plotted. The others are the same as in Fig. 6

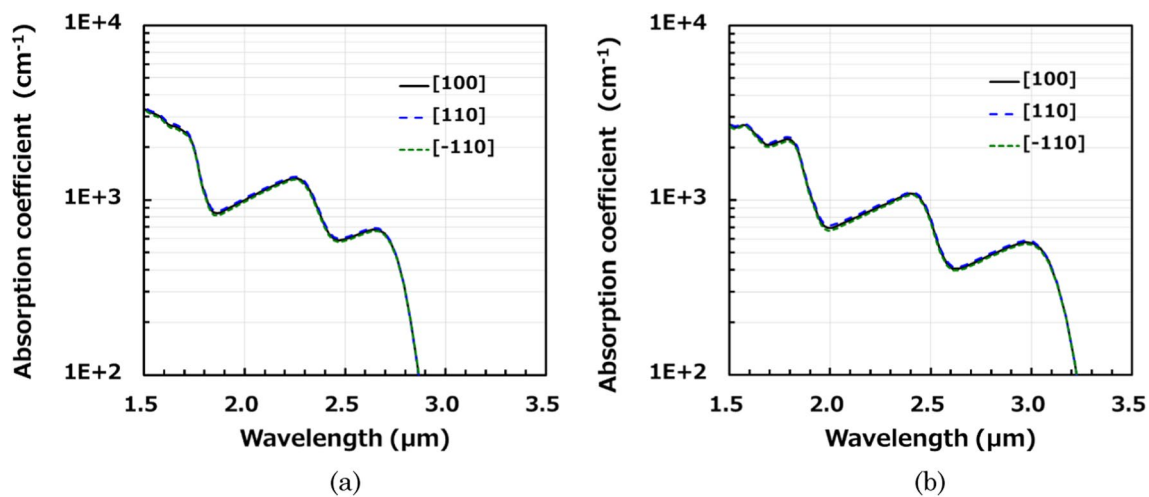


**Fig. 9** Dependences of the absorption coefficients on polarization direction in **a** SDA1 and **b** SDA2

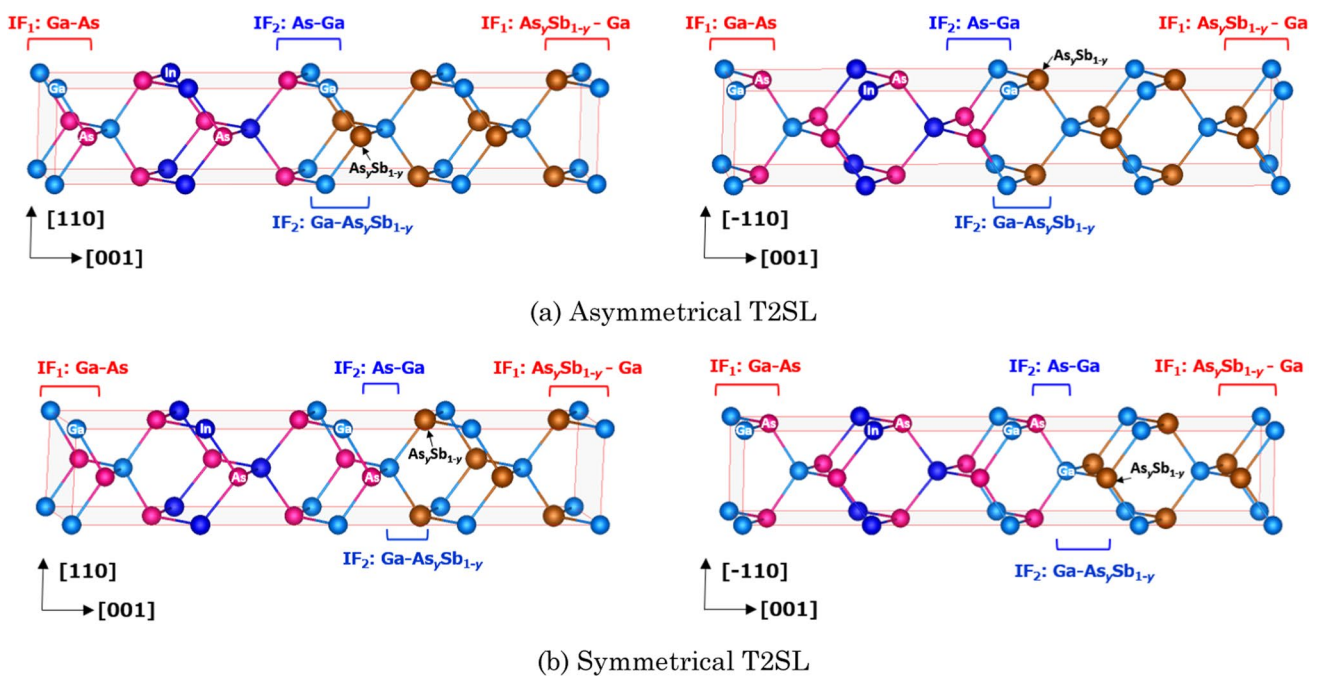


**Fig. 10** Illustrated atomic configurations of **a**  $(\text{GaAs})_2(\text{InAs})_2-(\text{GaAs}_y\text{Sb}_{1-y})_4$  and **b**  $(\text{GaAs})_2(\text{InAs})_2(\text{GaAs})-(\text{GaAs}_y\text{Sb}_{1-y})_3$  T2SLs, each of which is viewed from two different directions. The tetragonal

supercells overlap in these Figures. “ $\text{As}_y\text{Sb}_{1-y}$ ” denotes the anion atom of  $\text{GaAs}_y\text{Sb}_{1-y}$  in the TB scheme

supercells of the asymmetrical and the symmetrical T2SL, respectively. In the TB calculation of the optical absorption coefficient, the Peierls phase under long-wavelength approximation influences optical-transition-matrix elements as a factor  $\mathbf{r}_{c-a} \cdot \mathbf{e}_p$  [19], where  $\mathbf{r}_{c-a}$  is a vector connecting the positions of a cation and an anion atom, and  $\mathbf{e}_p$  is the unit vector of the electric field of the incident light. Thus, when the  $\mathbf{e}_p$  has a directional component of the

cation–anion bond (Ga–As, In–As, or Ga– $\text{As}_y\text{Sb}_{1-y}$ ), the interaction between the electric field of the incident light and the atomic bond contributes to the optical-transition-matrix elements. In the above notation of the Ga– $\text{As}_y\text{Sb}_{1-y}$  bond, “ $\text{As}_y\text{Sb}_{1-y}$ ” stands for the anion atom of  $\text{GaAs}_y\text{Sb}_{1-y}$  in the TB scheme. Note that, in each T2SL supercell, a number of the cation–anion bonds having directional components in the direction of polarization is the same for [110]

-polarization and  $[-110]$ -polarization (the number of bonds lying on the surface of the supercell is counted as half). Concretely, the number of the effective bonds having a directional component of  $[110]$  (or  $[-110]$ ) is written in parentheses next to each bond species as follows: Ga–As (4), In–As (4), and Ga–As<sub>y</sub>Sb<sub>1–y</sub> (8) are in the asymmetrical T2SL in Fig. 10a. Identically, Ga–As (6), In–As (4), and Ga–As<sub>y</sub>Sb<sub>1–y</sub> (6) are in the symmetrical T2SL in Fig. 10b. In the asymmetrical (GaAs)<sub>2</sub>(InAs)<sub>2</sub>–(GaAs<sub>y</sub>Sb<sub>1–y</sub>)<sub>4</sub> T2SL, being in a situation similar to the previously described asymmetrical wavefunction shape in DA2, since the CBM wavefunction is weighing to the IF<sub>2</sub> side, in the vicinity of the IF<sub>2</sub>, the electrons involved with the As–Ga–As<sub>y</sub>Sb<sub>1–y</sub> bonds having the directional component of  $e_p$  interact significantly with incident light. As can be seen from Fig. 10a, in the relationship between the atomic bond direction and the direction of  $e_p$ , near the IF<sub>2</sub>, the positions of As–Ga bonds having the  $[-110]$  component are closer to the electron well layer than the Ga–As<sub>y</sub>Sb<sub>1–y</sub> bonds with the  $[110]$  one. Namely, the CBM wavefunction more heavily influences the optical-transition-matrix elements involved with the former As–Ga bond. Considering this, it can be concluded that the incident light with  $[-110]$ -polarization interacts more strongly with the electrons in the As–Ga bonds close to the IF<sub>2</sub>. Therefore, it is reasonable that, in the absorption coefficient spectra of the asymmetrical digital T2SLs shown in Fig. 5a and b, the absorption coefficient of  $[-110]$ -polarization surpasses that of  $[110]$ -polarization. In the symmetrical T2SL, on the other hand, due to the symmetrical shape of the wavefunction, the bonds of Ga–As<sub>IF1</sub> and Ga–As<sub>y</sub>Sb<sub>1–y</sub><sub>IF2</sub> interact with  $[110]$ -polarized light in the same way that As–Ga<sub>IF2</sub> and As<sub>y</sub>Sb<sub>1–y</sub>–Ga<sub>IF1</sub> do with  $[-110]$ -polarized light, as illustrated in Fig. 10b. The above Ga–As<sub>IF1</sub> denotes the Ga–As bond near IF<sub>1</sub>; the notations of a bond near another interface denote likewise. Thus, it is sensible that in the symmetrical T2SLs, the absorption coefficient spectra shown in Fig. 9a and b vary little with alteration of the polarization direction of incident light.

Up to here, adopting simple digital alloy T2SL structures, we have shown the optical properties of (GaAs/InAs)–GaAs<sub>y</sub>Sb<sub>1–y</sub> digital alloy T2SLs. Lastly, this report investigates the feasibility of extending the wavelength region while maintaining a high absorption coefficient and examines several symmetrical digital alloy T2SLs satisfying the structure expression (1), finding that a [(GaAs)<sub>3</sub>(InAs)<sub>4</sub>(GaAs)<sub>4</sub>(InAs)<sub>4</sub>(GaAs)<sub>2</sub>]<sub>17</sub>–(GaAs<sub>0.50</sub>Sb<sub>0.50</sub>)<sub>17</sub> T2SL, as exhibited in Fig. 11, allows  $\lambda_g$  to lengthen considerably without seriously decreasing the absorption coefficient in the spectrum. Its  $\lambda_g$  indicates 2.86  $\mu\text{m}$  at  $T=200$  K, being longer over 0.4  $\mu\text{m}$  than in a conventional

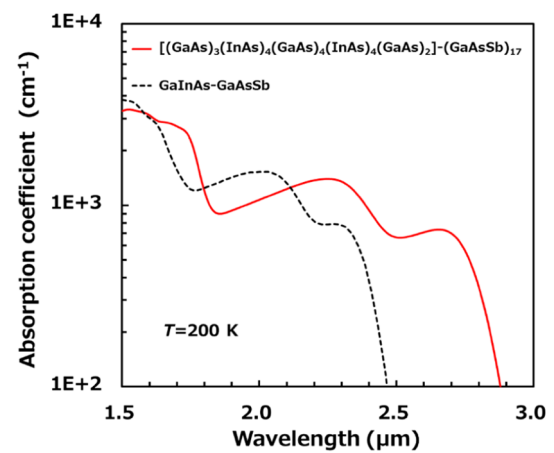


**Fig. 11** Absorption coefficient spectra of [(GaAs)<sub>3</sub>(InAs)<sub>4</sub>(GaAs)<sub>4</sub>(InAs)<sub>4</sub>(GaAs)<sub>2</sub>]<sub>17</sub>–(GaAs<sub>0.50</sub>Sb<sub>0.50</sub>)<sub>17</sub> and (Ga<sub>0.47</sub>In<sub>0.53</sub>As)<sub>17</sub>–(GaAs<sub>0.51</sub>Sb<sub>0.49</sub>)<sub>17</sub> T2SLs for  $[100]$ -polarized incident light

GaInAs–GaAsSb T2SL, which suggests that symmetrical digital alloy T2SLs are beneficial to significantly broaden the sensitivity region in SWIR detectors.

## 4 Conclusion

Aiming at the application of a digital alloy to an InP-based optical absorber in a SWIR detector, this study has revealed the optical properties of (GaAs/InAs)–GaAsSb digital alloy T2SLs for the first time by the empirical  $sp^3d^5s^*$  TB method. The digital alloy T2SL [(GaAs)<sub>3</sub>(InAs)<sub>4</sub>(GaAs)<sub>4</sub>(InAs)<sub>4</sub>(GaAs)<sub>2</sub>]<sub>17</sub>–(GaAs<sub>0.50</sub>Sb<sub>0.50</sub>)<sub>17</sub> has presented a  $\lambda_g$  of 2.9  $\mu\text{m}$  at  $T=200$  K; the  $\lambda_g$  is over 0.4  $\mu\text{m}$  longer than in a conventional GaInAs–GaAsSb T2SL, demonstrating the possible lengthening of the cut-off wavelength of the detector. Furthermore, this paper has shown the polarization-direction dependency of incident light in the absorption coefficient spectrum of asymmetrical (GaAs/InAs)–GaAsSb T2SLs arises from the asymmetric shape of the wavefunction (being attributed to the CBO profile); this dependency can be drastically decreased by modifying the configuration of the atomic layer in the growth direction to have mirror symmetry.

**Author contributions** The study of the methodology for the investigation and the analysis of the data were performed by TK and SS. The first draft of the manuscript was written by TK, and all authors commented on the previous versions of it. All authors read and approved the final manuscript.

**Funding** No funding was received to assist with the preparation of this manuscript.

**Data availability** All data generated or analyzed during this study are included in this published article.

## Declarations

**Conflict of interest** The authors have no competing interests to declare that are relevant to the content of this article.

## References

- M.P. Hansen, D.S. Malchow, Overview of SWIR detectors, cameras, and applications, In: *Proc. SPIE 6939, Thermosense XXX*, 69390I (2008). <https://doi.org/10.1117/12.777776>
- G.A. Tidhar, R. Segal, New applications with a SWIR imager employing long wavelengths, In: *Proceedings 8012, Infrared Technology and Applications XXXVII*; 801207 (2011). <https://doi.org/10.1117/12.884435>
- L.A. Sordillo, L. Shi, D.C. Sordillo, P.P. Sordillo, R.R. Alfano, Advances in medical applications using SWIR light in the wavelength range from 1000–2500 nm. In: *Proc. SPIE 10873, Optical Biopsy XVII: Toward Real-Time Spectroscopic Imaging and Diagnosis*, 108730T (2019). <https://doi.org/10.1117/12.2513382>
- L. G. Hipwood, N. Shorrocks, C. Maxey, D. Atkinson, N. Bezawada, SWIR and NIR MCT arrays grown by MOVPE for astronomy applications. In: *Proc. SPIE 8353, Infrared Technology and Applications XXXVIII*, 83532M (2012). <https://doi.org/10.1117/12.919007>
- A. Rogalski, Competitive technologies of third generation infrared photon detectors. *Opto Electron. Rev.* **14**, 84–98 (2006). <https://doi.org/10.2478/s11772-006-0012-2>
- A. Rogalski, Infrared detectors for the future. *Acta Physica Polonica A* **116**, 389–406 (2009). <https://doi.org/10.12693/APhysPolA.116.389>
- H. Yuan, J. Zhang, J. Kim, D. Bond, J. Laquindanum, J. Kimchi, M.G. DeForest, Recent progress in extended wavelength InGaAs photodetectors and comparison with SWIR HgCdTe photodetectors, In: *Proc. SPIE 11129, Infrared Sensors, Devices, and Applications IX*, 111290E (2019). <https://doi.org/10.1117/12.2532418>
- R. Sidhu, Ning Duan, J. C. Campbell, A. L. Holmes, A long-wavelength photodiode on InP using lattice-matched GaInAs-GaAsSb type-II quantum wells, *IEEE Photon. Technol. Lett.* **17**, 2715–2717 (2005). <https://doi.org/10.1109/LPT.2005.859163>.
- Y. Uliel, D. Cohen-Elias, N. Siconolfi, I. Grimberg, N. Snapi, Y. Paltiel, M. Katz, InGaAs/GaAsSb Type-II superlattice based photodiodes for short wave infrared detection. *Infrared Phys. Technol.* **84**, 63–71 (2017). <https://doi.org/10.1016/j.infrared.2017.02.003>
- K. Fujii, T. Ishizuka, Y. Nagai, Y. Iguchi, K. Akita, MOVPE growth for photodiodes in 2.5  $\mu\text{m}$  region with InGaAs/GaAsSb type-II quantum wells. *Phys. Status Solidi, C* **10**, 732–735 (2013). <https://doi.org/10.1002/pssc.201200611>
- R. Sidhu, N. Duan, J. C. Campbell, A. L. Holmes, A 2.3  $\mu\text{m}$  cut-off wavelength photodiode on InP using lattice-matched GaInAs-GaAsSb type-II quantum wells. In: *International Conference on Indium Phosphide and Related Materials, 2005, Glasgow, UK*, pp. 148–151 2005. <https://doi.org/10.1109/ICIPRM.2005.1517441>
- S.Z. Ahmed, Y. Tan, J. Zheng, J.C. Campbell, A.W. Ghosh, Atomistic transport modeling, design principles, and empirical rules for low-noise III–V digital-alloy avalanche photodiodes. *Phys. Rev. Appl.* **17**, 034044 (2022). <https://doi.org/10.1103/PhysRevApplied.17.034044>
- J. Zheng, Y. Yuan, Y. Tan, Y. Peng, A.K. Rockwell, S.R. Bank, A.W. Ghosh, J.C. Campbell, Digital alloy InAlAs avalanche photodiodes. *J. Lightwave Technol.* **36**, 3580–3585 (2018). <https://doi.org/10.1109/JLT.2018.2844114>
- A.K. Rockwell, M. Ren, M. Woodson, A.H. Jones, S.D. March, Y. Tan, Y. Yuan, Y. Sun, R. Hool, S.J. Maddox, M.L. Lee, A.W. Ghosh, J.C. Campbell, S.R. Bank, Toward deterministic construction of low noise avalanche photodetector materials. *Appl. Phys. Lett.* **113**, 102106 (2018). <https://doi.org/10.1063/1.5040592>
- R. Magri, A. Zunger, Effects of interfacial atomic segregation and intermixing on the electronic properties of InAs/GaSb superlattices. *Phys. Rev. B* **65**, 165302 (2002). <https://doi.org/10.1103/PhysRevB.65.165302>
- A. Sawamura, T. Kato, S. Souma, Improved tight-binding parameters of III–V semiconductor alloys and their application to type-II superlattices, *Jpn. J. Appl. Phys.* **61**, 021004 (2022). <https://doi.org/10.35848/1347-4065/ac4463>
- J. Otsuka, T. Kato, H. Sakakibara, T. Kotani, Band structures for short-period  $(\text{InAs})_n(\text{GaSb})_n$  superlattices calculated by the quasiparticle self-consistent GW method. *Jpn. J. Appl. Phys.* **56**, 021201 (2017). <https://doi.org/10.7567/JJAP.56.021201>
- S.Y. Ren, J.D. Dow, D.J. Wolford, Pressure dependence of deep levels in GaAs. *Phys. Rev. B* **25**, 7661 (1982). <https://doi.org/10.1103/PhysRevB.25.7661>
- A. Mehdipour, K. Sasaoka, M. Ogawa, S. Souma, Strain-induced modulation of anisotropic photoconductivity in graphene. *Jpn. J. Appl. Phys.* **53**, 115103 (2014). <https://doi.org/10.7567/JJAP.53.115103>

**Publisher's Note** Springer Nature remains neutral with regard to jurisdictional claims in published maps and institutional affiliations.

Springer Nature or its licensor (e.g. a society or other partner) holds exclusive rights to this article under a publishing agreement with the author(s) or other rightsholder(s); author self-archiving of the accepted manuscript version of this article is solely governed by the terms of such publishing agreement and applicable law.